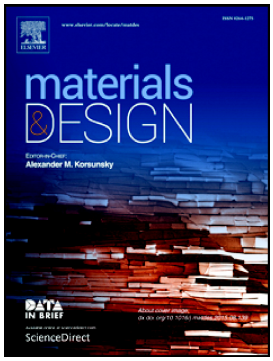

Combinational processing of 3D printing and electrospinning of hierarchical poly(lactic acid)/gelatin-forsterite scaffolds as a biocomposite: Mechanical and biological assessment

Saman Naghieh, Ehsan Foroozmehr, Mohsen Badrossamay, Mahshid Kharaziha

PII: S0264-1275(17)30720-7
DOI: doi: 10.1016/j.matdes.2017.07.051
Reference: JMADE 3241

To appear in: *Materials & Design*

Received date: 9 June 2017
Revised date: 14 July 2017
Accepted date: 24 July 2017

Please cite this article as: Saman Naghieh, Ehsan Foroozmehr, Mohsen Badrossamay, Mahshid Kharaziha , Combinational processing of 3D printing and electrospinning of hierarchical poly(lactic acid)/gelatin-forsterite scaffolds as a biocomposite: Mechanical and biological assessment, *Materials & Design* (2017), doi: 10.1016/j.matdes.2017.07.051

Combinational processing of 3D printing and electrospinning of hierarchical poly(lactic acid)/gelatin-forsterite scaffolds as a biocomposite: Mechanical and biological assessment

Saman Naghieh [1, 2], Ehsan Foroozmehr [2] *, Mohsen Badrossamay [2], Mahshid Kharaziha [3]

[1] Division of Biomedical Engineering, College of Engineering, University of Saskatchewan, Saskatoon, SK, Canada
[2] Department of Mechanical Engineering, Isfahan University of Technology, 8415683111, Isfahan, Iran
[3] Department of Materials Engineering, Isfahan University of Technology, 8415683111, Isfahan, Iran

Abstract: In this research, hierarchical scaffolds including poly(lactic acid) (PLA) micro struts and nanocomposite gelatin-forsterite fibrous layers were developed using fused deposition modeling (FDM) and electrospinning (ES), respectively. Briefly, geometrically various groups of pure PLA scaffolds (interconnected pores of 230 to 390 μm) were fabricated using FDM technique. After mechanical evaluation, ES technique was utilized to develop gelatin-forsterite nanofibrous layer. To study these scaffolds, scanning electron microscopy (SEM), Fourier transform infrared spectroscopy, and uniaxial compression tests were performed. Furthermore, bioactivity of the scaffolds was evaluated by immersing in the simulated body fluid and apatite formation on the surface of the scaffolds was investigated. Results depicted that elastic modulus of PLA/gelatin-forsterite scaffolds, fabricated by a combinational approach, was significantly higher than that of pure one (about 52%). SEM images showed the formation of calcium phosphate-like precipitates on the surface of these scaffolds, confirming the effects of nanocomposite fibrous layer on the improved bioactivity of the scaffolds. Regarding the obtained biological as well as mechanical properties, the developed bio-composite scaffolds can be used as a biocompatible candidate for bone tissue regeneration.

Keywords: 3D printing; Electrospinning; Bio-composite scaffold; Poly(lactic acid); Gelatin; Forsterite

1. Introduction

Tissue engineering is a multidisciplinary field including the combination of engineering and life science in order to provide a suitable structural framework to restore, protect, or augment the tissue functions [1]. From tissue engineering point of view, three-dimensional (3D) biocompatible scaffolds needed for bone regeneration have to mimic both biological and mechanical properties of the extracellular matrix (ECM) in order to control the cell function, diffusive capability and induce bone regeneration [2]. Furthermore, high diffusivity is necessary for 3D scaffolds in order to facilitate the mass transport of oxygen and nutrients [3,4]. To access this approach, the average pore size of scaffolds should be in the range of 300-400 μm to allow growing of the osteons into the scaffold [5]. In this regard, a complete library for engineered scaffold structures and their features was reported by Cheah et al. [6,7].

There are several techniques applied to fabricate 3D scaffolds such as fiber bonding [8], particular leaching [9] and emulsion freeze-drying [10]. Despite the promising results from

* Corresponding author; eforoozmehr@cc.iut.ac.ir; Tel. +98 31 3391 5238, Fax: +98 31 3391 2628

each technique, they indicate limitations consisting of uncontrollable architecture and lack of ability to control pore size and interconnectivity [11]. Other modern techniques developed for the fabrication of 3D scaffolds are additive manufacturing (AM) or rapid prototyping (RP) techniques [4,12]. These techniques are based on joining materials via layer by layer approach. They have undoubtedly revolutionized the fabrication of scaffolds by improving the ability to control pore size and interconnectivity [13]. These 3D scaffolds have been widely applied for various biomedical applications [14,15].

According to working principal, AM processes are divided into seven sub-groups of powder bed fusion, extrusion-based, material jetting, binder jetting, sheet lamination, directed energy deposition, and vat photo-polymerization processes [16]. FDM is one of the simplest and lowest cost methods [14], which is based on thermoplastic material deposition onto a platform [17]. FDM technique causes a noteworthy improvement in the quality of scaffold's constructs [18] and it can be used for a range of plastics [19]. Although FDM method has undeniable profits like eliminating the solvent from the fabrication process and possibility of vast material selection, it has some drawbacks like large pore sizes [20,21]. In order to overcome these issues, FDM technique has been combined with conventional techniques such as electrospinning (ES) and freeze-drying [22,23]. In this way, in order to mimic the ECM matrix, FDM technique has recently been combined with ES to develop scaffolds having the benefits of various kinds of materials just in one construction [13,24]. ES technique has been considered as an old technique to develop highly porous and fibrous scaffolds [25]. This method has the ability to control the morphology and diameter of fibers in the range of several micro to nanometers. The combination of AM and ES was the first effort to develop scaffolds with both micro- and nano-fibers [26]. For instance, Chen et al. [27] combined ES and FDM techniques for the fabrication of heart valve scaffold with desired physical and mechanical features.

Various types of polymers have been applied to develop 3D scaffolds bone tissue engineering applications. Amongst them, poly(lactic acid) (PLA) is a conventional and environmentally friendly thermoplastic polymer which belongs to the family of polyesters [28]. Recently, PLA scaffold has been developed using FDM approach [16,17,24,29,30]. For instance, Whulanza et al. developed PLA-gelatin scaffold using FDM approach for bone tissue engineering and showed that it can be used for direct cell incorporation in PLA scaffold [31]. However, the weak hydrophilicity of this polymer should be overcome via various physical or chemical methods [32,33]. The combination of synthetic polymers with natural polymers and bioactive ceramics is a promising approach developing scaffolds with improved mechanical and biological properties [34,35]. As an example, the fabrication of polymer-based composite scaffolds for bone tissue engineering has been reported elsewhere [12]. As another potential biomaterial, gelatin, derived from collagens, is a natural polymer which is highly applicable in tissue engineering due to its lower cost and relatively low antigenicity rather than collagen [34,36,37]. Recently, gelatin has been widely applied in combination with synthetic polymers such as polycaprolactone (PCL) and bioactive ceramics to promote biological properties for bone tissue engineering applications [24,35]. Between bioactive ceramics, forsterite (Mg_2SiO_4) has been introduced as novel bioceramics with interesting mechanical and biological properties [38,39]. Compared to other conventional bioactive ceramics such as hydroxyapatite and bioactive glass, forsterite shows significantly higher fracture toughness, superior to the lower limit reported for cortical bone [40,41]. These properties make it suitable for bone tissue engineering applications [39,42,43].

The aim of this study was to develop scaffolds of PLA/gelatin-forsterite using layer by layer FDM and ES techniques. The importance of the fabrication of bio-composites has been

highlighted elsewhere [44,45]. To the best of authors' knowledge, this is the first study presenting a fabrication method based on ES and FDM together considering a combination of PLA, gelatin, and forsterite. It was hypothesized that such a composition can satisfy both of mechanical (e.g. proper elastic modulus) and biological (e.g. bioactivity) requirements of scaffolds for bone tissue regeneration. For this purpose, micro-struts of PLA and nanocomposite gelatin-forsterite fibrous layers were fabricated using FDM and ES techniques together, respectively. It was supposed that adding gelatin-forsterite nanocomposite fibrous layers could improve the bioactivity and mechanical properties compared to pure PLA scaffold.

2. Materials and Methods

2.1. Materials

Gelatin (Type-A gelatin from bovine skin), acetic acid and N,N-(3-dimethylaminopropyl)- N'-ethyl-carbodiimide hydrochloride (EDC) were purchased from Sigma Company. Forsterite nanopowder (particle size = 25–45 nm) was synthesized by sol–gel method according to our previously reported procedures [39]. PLA (translucent, clear) was also supplied by Bits from Bytes (Clevedon, UK) as a 2.7 mm diameter filament for both scaffolds. The PLA polymer filaments applied in the fabrication process of scaffolds had T_g, T_c and T_m 62℃, 112℃, and 170℃, respectively.

2.2. Design and fabrication of pure scaffolds

Pure PLA scaffold was developed using FDM technique and in order to evaluate the effects of pore size and shape on the characteristics of scaffolds, three different groups were designed using G-Code program and named with S_1, S_2, and S_3 symbols. For bone tissue regeneration, scaffolds with 50 µm to 500 µm pore size have been reported [3]. The details of 3D-printing conditions are presented in Table 1. The generated G-code data was transferred to FDM machine. All scaffolds were fabricated by RAPMAN 3.2 (Clevedon, UK) with double nozzle head supplied by Bits from Bytes (Figure 1). The nozzle temperature was adjusted to 195 and 210 ℃ with respect to the sample. Moreover, the amount of layer thickness was set at 0.5 mm in the G-Code program. Additionally, the scaffolds were designed with 0-90 lay down pattern and fabricated in 35×35×4 mm^3 sizes.

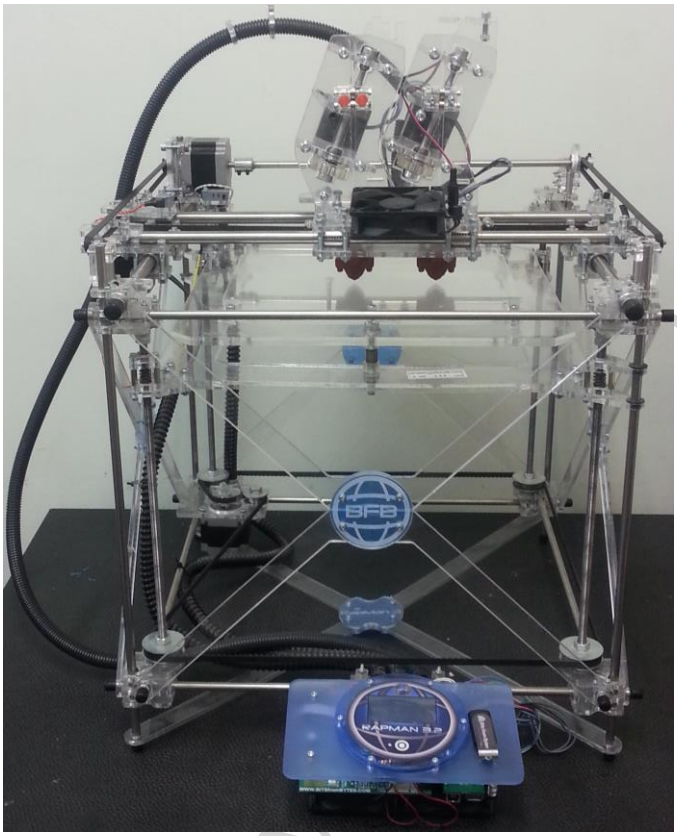

Figure 1. The FDM machine (Rapman 3.2) used to fabricate PLA scaffolds

Table 1. Details of the 3D-printing conditions in FDM machine

Samples	Liquefier temperature (℃)	Filament feed rate (RPM)	Head speed (mm/s)
S_1	210	10	6
S_2	210	20	7
S_3	195	10	5

According to Zein et al. [46], liquefier temperature and filament feed rate are factors which have a direct correlation with the consistency of the material flow for fabricating porous structures. Hence, all parameters were selected based on these pivotal factors. In addition, head speed was selected for reducing the fabrication time as well as having well-organized structures.

2.3. Development of PLA/gelatin-forsterite scaffolds using FDM and ES techniques

Scaffolds were developed via the addition of nanocomposite fibrous gelatin-forsterite layers via electrospinning technique, after every two layers of PLA microfibers (Figure 2). For this purpose, after fabrication of the first and second layers of PLA scaffold by FDM

machine, nanocomposite gelatin-forsterite fibrous layer was electrospun on the top of the scaffold.

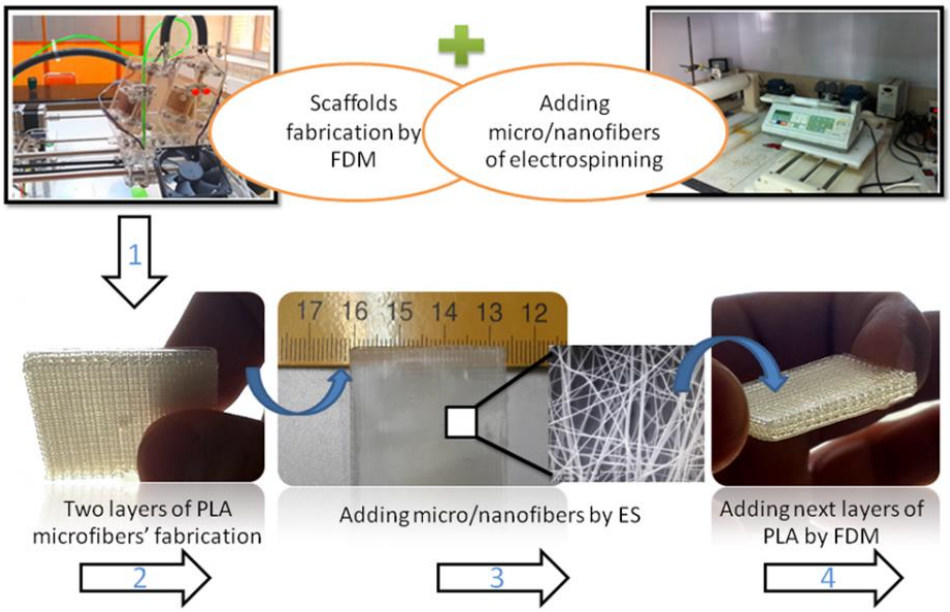

Figure 2. The production procedure of scaffold, fabricated using a combinational approach, including 1,2) fabrication of first and second layers of PLA using FDM, 3) adding micro/nanofibers using ES, 4) adding next layers of PLA using FDM technique

For the electrospinning process, gelatin-forsterite suspension consisting of 10%(w/v) forsterite nanopowder was prepared in a 10 %(w/v) gelatin solution in 80% (v/v) acetic acid mixture. After 1h sonication, the suspension was fed into 1 mL standard syringes equipped with a 23G blunted stainless steel needle using a syringe under the optimized ES parameters consisting 1 ml/h flow rate, 18 cm working distance (the distance between the collector and needle) and 17 kV voltage. Fibers were collected on the fabricated PLA scaffolds attached to the aluminum foil and kept for 24 h at room temperature in a vacuum desiccator to remove any residual solvent. This trend was repeated, subsequently, until the thickness of scaffolds was reached to 4 mm.

Due to rapid degradation of gelatin at a wet condition, crosslinking should be performed. For the crosslinking process, scaffolds were immersed in 75 mM EDC in 90% (v/v) ethanol solution for 12 h at 4 ℃. Finally, the crosslinked scaffolds were washed with phosphate buffered saline (PBS) to remove the residual of the crosslinking agent.

2.4. Scaffold characterization

The particle size morphology and distribution of forsterite nanopowder was determined using transmission electron microscopy (TEM). The chemical composition of the applied PLA and nanocomposite fibrous gelatin-forsterite were also confirmed through Fourier transform infrared spectroscopy (FTIR) (Bomem, MB 100) performed over a range of 600–4000 cm^{-1} and resolution of 2 cm^{-1}.

The porosity of scaffolds was evaluated using Archimedes approach based on the following equations [47]:

$$P = \frac{V(pore)}{V(pore) + V(scaffold)} \quad (1)$$

$$V(pore) = \frac{Md - Msw}{The\ density\ of\ ethanol} \quad (2)$$

$$V(scaffold) = \frac{Md}{Density\ of\ the\ PLA} \quad (3)$$

Where M_d is the mass of dry scaffolds, M_{sw} is the mass of the scaffolds swollen in ethanol, V(pore) is the amount of ethanol filled the open pores and V(scaffold) is the volume of the scaffold taken by the polymer. The density of the PLA was 1.17 gr/cm^3 and for ethanol was 0.807 gr/ cm^3. All the masses were measured via RADWAG® (AS 220/C/2) balance with 0.1 mg accuracy.

The morphology of the scaffolds was evaluated using scanning electron microscopy (SEM) (Philips XL30). Before imaging, the samples were gold-coated using sputter-coater. Additionally, SEM images were imported into Image J® 1.48v software (National Institute of Health, USA) and the fiber (n=40), strut diameter (n=40), and the pore size of the fabricated scaffolds were estimated.

The mechanical properties of the scaffolds were determined using compression test using Hounsfield (H50KS, Shakopee, USA) machine with preload of 1.5 N (load cell with the capacity of more than 5KN). According to ISO 604/B/1 [48], samples were cut into 10 × 10 × 3 mm^3 right prism shapes. The compression speed was set to 1 mm/min and after setting up compression plate, the compression load was fixed to zero every time.

Bioactivity of scaffolds, fabricated using FDM and ES, was also investigated using immersing into (SBF) prepared according to Kokubo protocol [49]. The samples with dimensions of 10×10×3 mm^3 were put in the polyethylene containers and kept at 37 °C for a month. The formation of apatite layer on the scaffolds, fabricated using the combinational approach, was confirmed using SEM imaging.

3. Results and discussion

SEM images were also utilized to determine the morphology as well as strut diameter and pore size of the samples (Figure 3). According to the side view of the sample S_3 (Figure 3(d)), presented as an example, all samples had rectangular-shaped interconnected pores. The average strut diameter and pore size mean values, in X and Y directions, of scaffolds were estimated from SEM images and presented in Table 2.

Table 2. Physical and mechanical properties of sample S_1, S_2 and S_3

Sample	Strut diameter (μm)	Pore size (mean values ±SD) (μm)		Porosity (%)	Elastic modulus (MPa)
		X direction	Y direction		
S_1	780±5	310±3	390±6	36.2±0.6	121.54±37.89
S_2	820±8	230±5	400±4	34.1±0.8	153.60±37.9
S_3	540±4	330±3	360±4	39.2±0.8	112.08±29.6

Between various scaffolds, sample S_2 revealed the largest struts (820±8 μm), while its pore size distribution in the X-direction was the least (230±5 μm vs 310±3 μm (at S1 sample) and 330±3 μm (at S3 sample)). These larger struts are due to using higher feed rate during the printing process. Sample S_2 shows largest struts, 820±8 μm, whereas samples S_1 and S_3 that contain smaller ones with 780±5 and 540±4 μm, respectively. In terms of the pore size, sample S_2 contains more rectangular shape pores than square one. The pores in this sample were around 230 x 400 μm. The pores of the S_1 sample were about 310 x 390 micron and the ones of S_3 were about 330 x 360 μm (the size with the most possibility were selected). Therefore, sample S_3 contained more uniform pores than the other two samples. Liquefier temperature and filament feed rate are factors that are responsible for theses changes in the morphology of scaffolds. Moreover, nozzle speed in X and Y directions could have a decisive role affecting the struts' diameter. Considering the proper pore size for osteons which is 300 to 400 μm [5], sample S_2 could not be a good candidate. Sample S_3 had a priority over sample S_1 due to its uniform distribution of pore sizes. Therefore, S_3 was the sample selected for the fabrication of scaffold, fabricated using FDM and ES. Moreover, based on equations (1), (2), and (3), the average porosity of samples was calculated about 36.2±0.6%, 34.1±0.8%, and 39.2±0.8% for S_1, S_2, and S_3 samples, respectively. It is worth mentioning that all the fabrication parameters of scaffolds, in this study, were selected based on pivotal factors of feed rate and head temperature, and proper pore size for osteons, according to literature. Moreover, head speed was selected for reducing the fabrication time as well as having well-organized structures. In the extrusion-based technique, the optimized head speed can be estimated based on the flow rate of the material depending on viscosity, flow consistency, etc. [50].

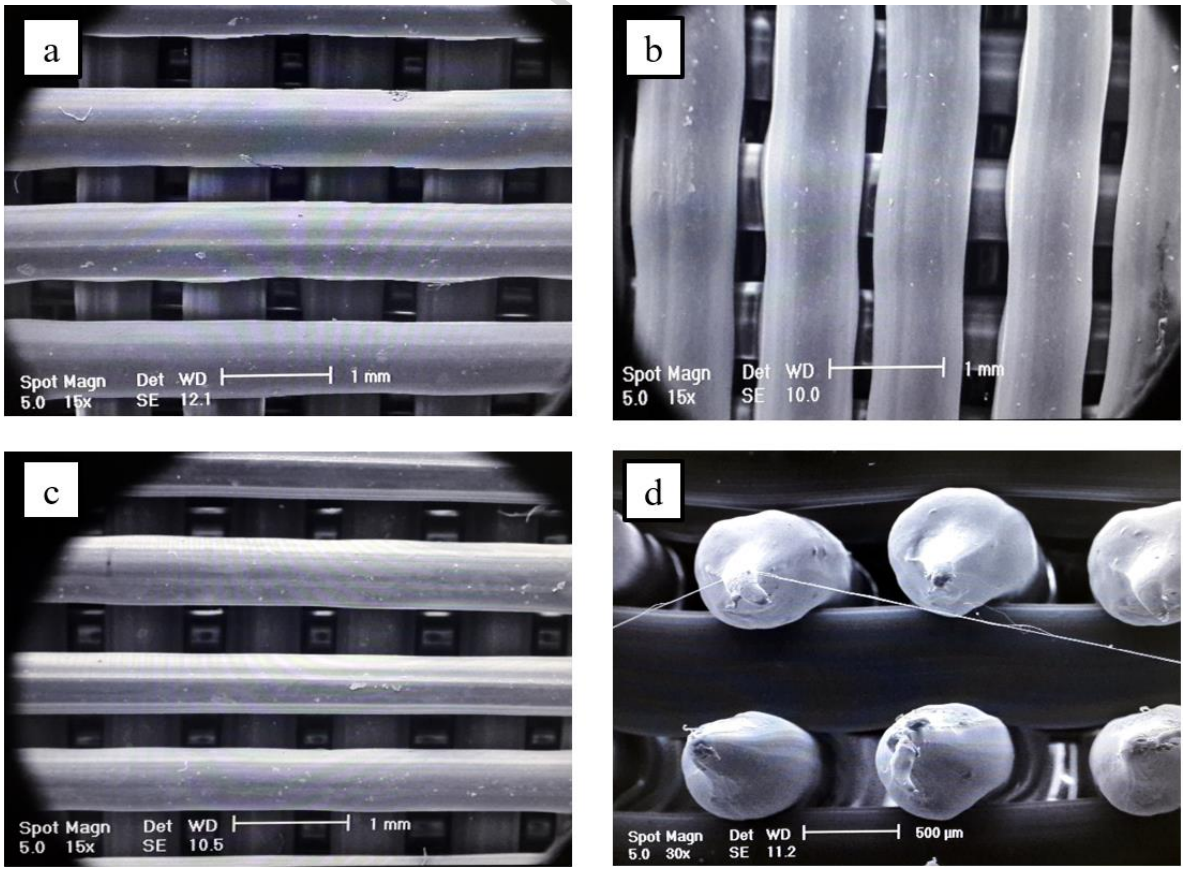

Figure 3. Characterization of the PLA scaffolds: SEM images of a) S_1, b) S_2, c) S_3 samples, and d) the cross view the S_3

It was reported that a huge difference between the elastic modulus of the scaffold and natural bone can cause some issues like stress shielding [51]. Mechanical properties of the samples were evaluated using compression test (Figure 4). Based on ASTM D695 [52], the elastic modulus of each sample was calculated. All samples present a non-linear behavior at the beginning, followed by a relatively linear trend, and finished by a semi-plateau reaction. The linear section was considered for the calculation of the elastic modulus. As it was reported in Table 2, the average value of the elastic modulus of sample S_1, S_2 and S_3 were 121.54±37.89 MPa, 153.60±37.9 MPa and 112.08±29.6 MPa, respectively. It should be noted that the elastic modulus of PLA scaffolds was dependent on the molecular weight and the degree of crystallinity of the PLA [53,54]. Hence, different PLA materials with various molecular weight and degree of crystallinity can result in different mechanical properties. With respect to the obtained values, sample S_2 had the higher mechanical properties, resulting from larger struts diameter and less average pore size than two other samples (S_1 and S_3). However, considering the large deviations of the results, the Student's t-test did not confirm a meaningful difference. It might be due to the anisotropic characteristics of FDM parts with respect to various reports about the influence of directionally-dependent techniques like FDM as it was reported by Ziemian, et al. [55]. It should be noted that in the most majority of studies related to bone tissue engineering, the emphasis is put on elastic modulus due to issues related to stress-shielding phenomenon. For instance, Ostrowska et al. reported 5.4 MPa as the elastic modulus of scaffolds, fabricated using FDM and ES, including PCL micro struts in addition to PLLA nano fibers [56]. In other studies, 2.05 MPa and 9.68 MPa were reported as the elastic modulus of PCL-based scaffolds, fabricated using a combinational approach [21,57]. However, the elastic modulus of cancellous bone is between 10 to 2000 Mpa, according to [56]. Therefore, the aforementioned scaffolds have lower elastic modulus rather than the cancellous bone and, thus, scaffolds with higher elastic modulus are required. To address this issue, in this study, parameters were selected so that higher elastic modulus was achieved.

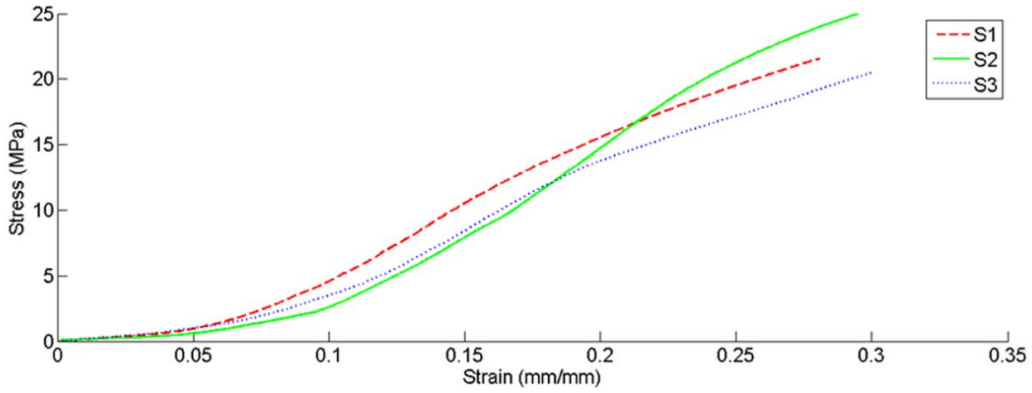

Figure 4. Stress-strain curves of compression tests performed on PLA samples

After optimization of FDM parameters and selection of sample S_3 as the optimized scaffold, layer by layer process was performed using FDM technique followed by ES process in order to develop scaffolds using this combinational approach. SEM images of this scaffold are presented in Figure 5(a) and (b) as secondary and backscatter modes, respectively. Electrospun fibers distributed throughout the surface of micro PLA struts and covered the entire strut's surface properly. High magnification image of nanocomposite gelatin-forsterite

fibrous scaffold (Figure 5(c)) revealed the formation of uniform and bead-free fibers with the average size of 580±160 µm. Moreover, forsterite nanopowder with the particle size of 25-45 nm and spherical shapes (inset in Figure 5(c)) was uniformly dispersed within gelatin matrix without any agglomeration. FTIR spectrum of nanocomposite gelatin-forsterite fibrous layer (Figure 5(d)) also demonstrated the presence of gelatin and forsterite nanopowder. The spectrum consisted of the characteristic peaks of gelatin at 1650 cm^{-1} (C=O stretching), 1550 cm^{-1} (N-H bend and C-H stretching), 1267 cm^{-1} (N-H stretching) and 3300 cm^{-1} (N-H stretching vibration), corresponding to amide I, amide II, amide III and amide A peak, respectively. Furthermore, the characteristic absorption bands of forsterite at 830–1000 cm^{-1} related to the various vibration modes of Si-O-Si bonds were observed confirming the presence of forsterite within gelatin matrix.

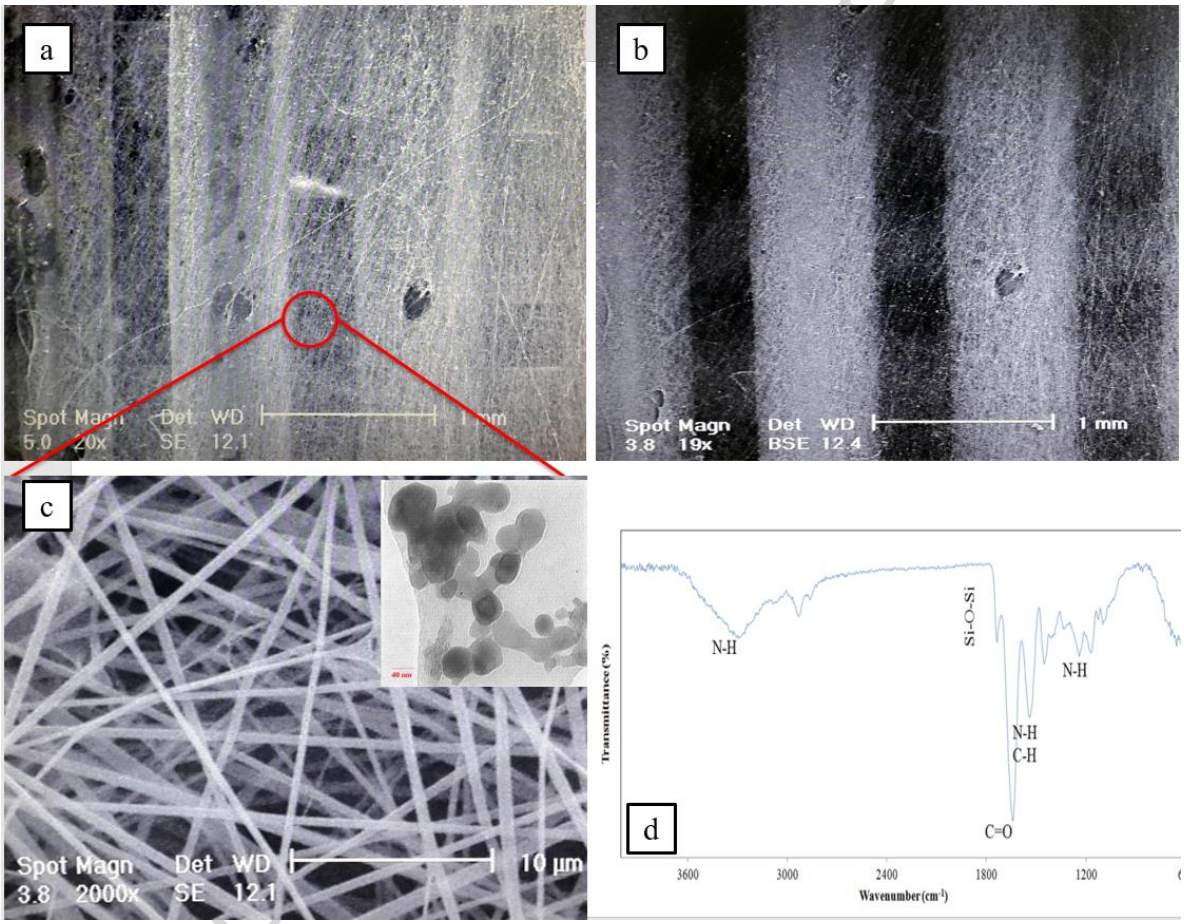

Figure 5. Characterization of PLA/gelatin-forsterite scaffolds: SEM images **(**a) Secondary and b) backscatter modes**)** of the PLA/gelatin-forsterite scaffold, c) SEM images of nanocomposite gelatin-forsterite fibrous layer (inset is the TEM micrograph of the forsterite nanopowders), d) FTIR spectrum of the nanocomposite gelatin-forsterite fibrous layer

The stress-strain curve of the PLA/gelatin-forsterite scaffold is shown in Figure 6. The elastic modulus of this scaffold was 170.3±13.9 MPa which was more than that of pure PLA one (112.08±29.6 MPa). However, it was reported that the addition of nanofibers using ES technique to the struts of the additive manufactured scaffolds decreases the compressive elastic modulus of the scaffold, fabricated using FDM and ES, rather than the additive manufactured one [21,56]. Our results showed that the scaffolds, fabricated using the proposed combinational approach, had more elastic modulus rather than the pure ones. It might be because of the presence of forsterite nanopowder to the gelatin matrix. It was

reported that the addition of nanoparticles to the polymeric structure could enhance the mechanical properties [58]. Furthermore, nanocomposite fibrous layer may increase the effective surface of the previous layer, resulting in better attachment of the next PLA deposition. It can be concluded that the incorporation of the gelatin-forsterite nanocomposite fibrous layer not only reduced pore size but also could enhance the mechanical properties of the scaffolds.

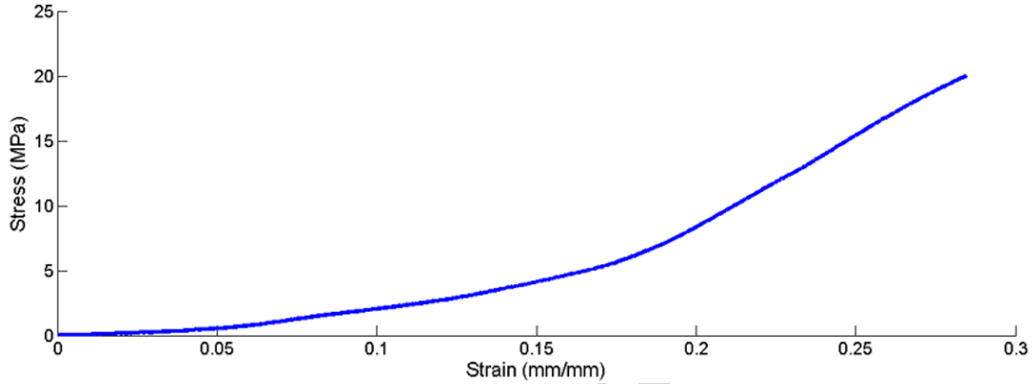

Figure 6. Stress-strain of PLA/gelatin-forsterite scaffold

The ability of PLA/gelatin-forsterite scaffolds in the formation of bone-like apatite on the scaffold surface was evaluated using soaking in SBF solution. SEM images of these scaffolds after immersion in SBF for 28 days are shown in Figure 7. It was observed that the struts of the scaffold were covered by hydroxyapatite (HA) crystals. This cover could be identified via famous cauliflower-like and globular shape of hydroxyapatite crystals confirming the bioactivity of these scaffolds.

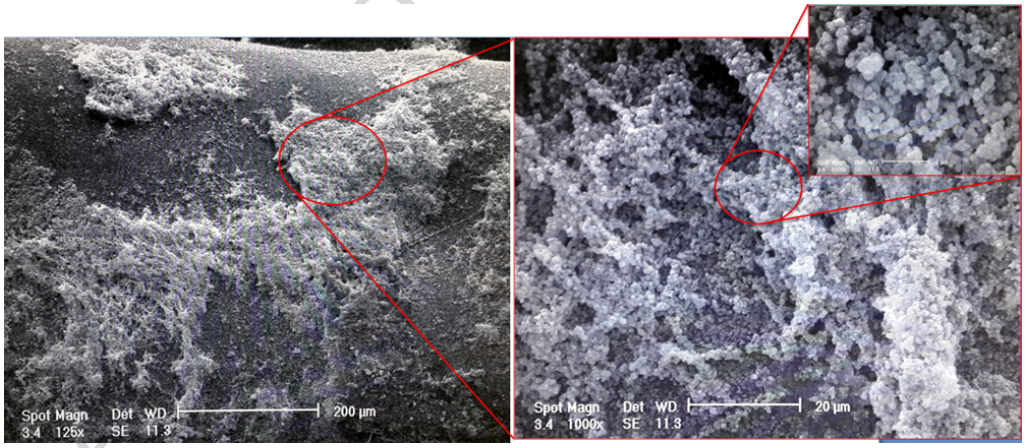

Figure 7. Representative SEM images of the PLA/gelatin-forsterite scaffolds after immersion in SBF for 28 days

It was reported that deposited crystals were not formed on the surface of pure PLA scaffold immersed in SBF for 35 weeks [54]. However, our results showed that the combination of PLA and gelatin-forsterite could provide a good substrate for HA deposition. This could be due to the presence of forsterite nanopowder and its role to have a bioactive scaffold. Recent results showed significantly higher potential of forsterite for in vivo bone formation than other bioactive ceramics such as bioactive glass [40,41]. Therefore, the presence of forsterite nanopowder within 3D scaffolds with appropriate pore size could provide a promising construct for bone tissue engineering application.

4. Conclusions

This study was focused on the development of novel scaffolds of PLA microfibers combined with nanocomposite gelatin-forsterite fibrous layer for bone tissue engineering application. The emphasis was put on the formation of PLA/gelatin-forsterite scaffold with lower pore size than that of PLA one, as the main novelty of this study. Results indicated that hierarchical scaffolds, fabricated using FDM and ES, revealed 52% increase in elastic modulus rather than the pure one owing to the presence of forsterite nanopowder incorporated within gelatin matrix. In addition, immersing the PLA/gelatin-forsterite scaffolds in SBF solution showed the significant formation of bone-like apatite on the surface of the struts. It was concluded that the proposed scaffolds, as a bio-composite fabricated using a combinational trend, provide appropriate mechanical and biological properties. Based on the achieved results, these scaffolds of PLA and gelatin-forsterite had appropriate mechanical and biological properties, so that it can be applied as a bioactive bone substitute in maxillofacial applications.

Acknowledgments: The authors gratefully thank Dr. Sahar Salehi for his appreciable consultations.

References

[1] R. Langer, Perspectives and challenges in tissue engineering and regenerative medicine, Adv. Mater. 21 (2009) 3235–3236.

[2] E. Boccardi, I. V Belova, G.E. Murch, A.R. Boccaccini, T. Fiedler, Oxygen diffusion in marine-derived tissue engineering scaffolds, J. Mater. Sci. Mater. Med. 26 (2015) 1–9.

[3] S. Yang, H. Yang, X. Chi, J.R.G. Evans, I. Thompson, R.J. Cook, P. Robinson, Rapid prototyping of ceramic lattices for hard tissue scaffolds, Mater. Des. 29 (2008) 1802–1809. doi:10.1016/j.matdes.2008.03.024.

[4] D.M. Correia, C. Ribeiro, V. Sencadas, L. Vikingsson, M.O. Gasch, J.L.G. Ribelles, G. Botelho, S. Lanceros-méndez, Strategies for the development of three dimensional scaffolds from piezoelectric poly (vinylidene fluoride), Mater. Des. 92 (2016) 674–681. doi:10.1016/j.matdes.2015.12.043.

[5] M.G. Yeo, G.H. Kim, Preparation and characterization of 3D composite scaffolds based on rapid-prototyped PCL/β-TCP struts and electrospun PCL coated with collagen and HA for bone regeneration, Chem. Mater. 24 (2011) 903–913.

[6] C.M. Cheah, C.K. Chua, K.F. Leong, S.W. Chua, Development of a tissue engineering scaffold structure library for rapid prototyping. Part 2: parametric library and assembly program, Int. J. Adv. Manuf. Technol. 21 (2003) 302–312.

[7] C.M. Cheah, C.K. Chua, K.F. Leong, S.W. Chua, Development of a tissue engineering scaffold structure library for rapid prototyping. Part 1: investigation and classification, Int. J. Adv. Manuf. Technol. 21 (2003) 291–301.

[8] A.G. Mikos, A.J. Thorsen, L.A. Czerwonka, Y. Bao, R. Langer, D.N. Winslow, J.P. Vacanti, Preparation and characterization of poly (L-lactic acid) foams, Polymer (Guildf). 35 (1994) 1068–1077.

[9] Q. Cai, J. Yang, J. Bei, S. Wang, A novel porous cells scaffold made of polylactide–dextran blend by combining phase-separation and particle-leaching techniques, Biomaterials. 23 (2002) 4483–4492.

[10] K.E. Healy, K. Whang, C.H. Thomas, Method of fabricating emulsion freeze-dried scaffold bodies and resulting products, 5,723,508, 1998.

[11] S.P.P. Poh, In vitro and in vivo assessment of bioactive composite scaffolds fabricated via additive manufacturing technology, Queensland University of Technology, 2014.

[12] E. Tamjid, A. Simchi, Fabrication of a highly ordered hierarchically designed porous nanocomposite via indirect 3D printing: Mechanical properties and in vitro cell responses, Mater. Des. 88 (2015) 924–931. doi:10.1016/j.matdes.2015.08.133.

[13] S.M. Giannitelli, P. Mozetic, M. Trombetta, A. Rainer, Combined additive manufacturing approaches in tissue engineering, Acta Biomater. 24 (2015) 1–11. doi:10.1016/j.actbio.2015.06.032.

[14] D.V. V Isakov, Q. Lei, F. Castles, C.J.J. Stevens, C.R.M.R.M. Grovenor, P.S.S. Grant, 3D printed anisotropic dielectric composite with meta-material features, Mater. Des. 93 (2016) 423–430. doi:10.1016/j.matdes.2015.12.176.

[15] L. Zhao, Z. Zhang, Y. Song, S. Liu, Y. Qi, X. Wang, Q. Wang, C. Cui, Mechanical properties and in vitro biodegradation of newly developed porous Zn scaffolds for biomedical applications, Mater. Des. 108 (2016) 136–144. doi:10.1016/j.matdes.2016.06.080.

[16] S. Naghieh, M.R. Karamooz Ravari, M. Badrossamay, E. Foroozmehr, M. Kadkhodaei, Numerical investigation of the mechanical properties of the additive manufactured bone scaffolds fabricated by FDM: the effect of layer penetration and post-heating, Mech. Behav. Biomed. Mater. 59 (2016) 241–250. doi:10.1016/j.jmbbm.2016.01.031.

[17] S. Naghieh, A. Reihany, A. Haghighat, E. Foroozmehr, M. Badrossamay, F. Forooghi, Fused Deposition Modeling and Fabrication of a Three-dimensional Model in Maxillofacial Reconstruction, Regen. Reconstr. Restor. 1 (2016) 139–144.

[18] M.E. Hoque, D.W. Hutmacher, W. Feng, S. Li, M.-H. Huang, M. Vert, Y.S. Wong, Fabrication using a rapid prototyping system and in vitro characterization of PEG-PCL-PLA scaffolds for tissue engineering, J. Biomater. Sci. Polym. Ed. 16 (2005) 1595–1610.

[19] M. Nikzad, S.H. Masood, I. Sbarski, Thermo-mechanical properties of a highly filled polymeric composites for fused deposition modeling, Mater. Des. 32 (2011) 3448–3456. doi:10.1016/j.matdes.2011.01.056.

[20] I. Zein, D.W. Hutmacher, K.C. Tan, S.H. Teoh, Fused deposition modeling of novel scaffold architectures for tissue engineering applications, Biomaterials. 23 (2002) 1169–1185. doi:10.1016/S0142-9612(01)00232-0.

[21] G. Kim, J. Son, S. Park, W. Kim, Hybrid process for fabricating 3D hierarchical scaffolds combining rapid prototyping and electrospinning, Macromol. Rapid Commun. 29 (2008) 1577–1581.

[22] D. Puppi, X. Zhang, L. Yang, F. Chiellini, X. Sun, E. Chiellini, Nano/microfibrous polymeric constructs loaded with bioactive agents and designed for tissue engineering applications: A review, J. Biomed. Mater. Res. Part B Appl. Biomater. 102 (2014) 1562–1579.

[23] L. Moroni, A. Nandakumar, F.B. Groot, C.A. Blitterswijk, P. Habibovic, Plug and play: combining materials and technologies to improve bone regenerative strategies, J. Tissue Eng. Regen. Med. (2013).

[24] S. Naghieh, M. Badrossamay, E. Foroozmehr, M. Kharaziha, Combination of PLA Micro-fibers and PCL-Gelatin Nano-fibers for Development of Bone Tissue Engineering Scaffolds, Int. J. Swarm Intell. Evol. Comput. 6 (2017) 1–4. doi:10.4172/2090-4908.1000150.

[25] L. Larrondo, R. St John Manley, Electrostatic fiber spinning from polymer melts. I. Experimental observations on fiber formation and properties, J. Polym. Sci. Polym. Phys. Ed. 19 (1981) 909–920.

[26] P.D. Dalton, C. Vaquette, B.L. Farrugia, T.R. Dargaville, T.D. Brown, D.W. Hutmacher, Electrospinning and additive manufacturing: converging technologies, Biomater. Sci. 1 (2013) 171–185.

[27] R. Chen, Y. Morsi, S. Patel, Q. Ke, X. Mo, A novel approach via combination of electrospinning and

FDM for tri-leaflet heart valve scaffold fabrication, Front. Mater. Sci. China. 3 (2009) 359–366.

[28] M. Murariu, A.-L. Dechief, R. Ramy-Ratiarison, Y. Paint, J.-M. Raquez, P. Dubois, Recent advances in production of poly (lactic acid)(PLA) nanocomposites: a versatile method to tune crystallization properties of PLA, Nanocomposites. 1 (2015) 71–82.

[29] S. Hsu, H. Yen, C. Tseng, C. Cheng, C. Tsai, Evaluation of the growth of chondrocytes and osteoblasts seeded into precision scaffolds fabricated by fused deposition manufacturing, J. Biomed. Mater. Res. Part B Appl. Biomater. 80 (2007) 519–527.

[30] D.W. Hutmacher, M. Sittinger, M. V Risbud, Scaffold-based tissue engineering: rationale for computer-aided design and solid free-form fabrication systems, Trends Biotechnol. 22 (2004) 354–362. doi:http://dx.doi.org/10.1016/j.tibtech.2004.05.005.

[31] Y. Whulanza, P. Hidayaturrahmi, T. Kurniawati, Realization and testing of multi-material 3D printer for bone scaffold fabrication, in: AIP Conf. Proc., AIP Publishing, 2017: p. 40001.

[32] V. Kudryavtseva, K. Stankevich, A. Gudima, E. Kibler, Y. Zhukov, E. Bolbasov, A. Malashicheva, M. Zhuravlev, V. Riabov, T. Liu, Atmospheric pressure plasma assisted immobilization of hyaluronic acid on tissue engineering PLA-based scaffolds and its effect on primary human macrophages, Mater. Des. (2017).

[33] K. Kim, M. Yu, X. Zong, J. Chiu, D. Fang, Y.-S. Seo, B.S. Hsiao, B. Chu, M. Hadjiargyrou, Control of degradation rate and hydrophilicity in electrospun non-woven poly (D, L-lactide) nanofiber scaffolds for biomedical applications, Biomaterials. 24 (2003) 4977–4985.

[34] M. Kharaziha, M.H. Fathi, H. Edris, Tunable cellular interactions and physical properties of nanofibrous PCL-forsterite: gelatin scaffold through sequential electrospinning, Compos. Sci. Technol. 87 (2013) 182–188.

[35] Y. Hosseini, R. Emadi, M. Kharaziha, Surface modification of PCL-diopside fibrous membrane via gelatin immobilization for bone tissue engineering, Mater. Chem. Phys. 194 (2017) 356–366.

[36] S. Kojima, T. Sugiyama, S. Takai, D. Jin, M. Ueki, H. Oku, Y. Tabata, T. Ikeda, Effects of Gelatin Hydrogel Loading Mitomycin C on Conjunctival Scarring in a Canine Filtration Surgery Model., Invest. Ophthalmol. Vis. Sci. 56 (2015) 2601–2605.

[37] X. Zhao, Q. Lang, L. Yildirimer, Z.Y. Lin, W. Cui, N. Annabi, K.W. Ng, M.R. Dokmeci, A.M. Ghaemmaghami, A. Khademhosseini, Photocrosslinkable Gelatin Hydrogel for Epidermal Tissue Engineering, Adv. Healthc. Mater. (2015) 1–11.

[38] M. Kharaziha, M.H. Fathi, Improvement of mechanical properties and biocompatibility of forsterite bioceramic addressed to bone tissue engineering materials, J. Mech. Behav. Biomed. Mater. 3 (2010) 530–537.

[39] M. Kharaziha, M.H. Fathi, Synthesis and characterization of bioactive forsterite nanopowder, Ceram. Int. 35 (2009) 2449–2454.

[40] M.H. Fathi, M. Kharaziha, Two-step sintering of dense, nanostructural forsterite, Mater. Lett. 63 (2009) 1455–1458.

[41] A. Forghani, M. Mapar, M. Kharaziha, M.H. Fathi, M. Fesharaki, Novel Fluorapatite- Forsterite Nanocomposite Powder for Oral Bone Defects, Int. J. Appl. Ceram. Technol. 10 (2013) E282–E289.

[42] M. Kharaziha, M.H. Fathi, H. Edris, Development of novel aligned nanofibrous composite membranes for guided bone regeneration, J. Mech. Behav. Biomed. Mater. 24 (2013) 9–20.

[43] R. Emadi, F. Tavangarian, S.I.R. Esfahani, A. Sheikhhosseini, M. Kharaziha, Nanostructured forsterite coating strengthens porous hydroxyapatite for bone tissue engineering, J. Am. Ceram. Soc. 93 (2010)

2679–2683.

[44] M.U. Jurczyk, K. Jurczyk, A. Miklaszewski, M. Jurczyk, Nanostructured titanium-45S5 Bioglass scaffold composites for medical applications, Mater. Des. 32 (2011) 4882–4889. doi:10.1016/j.matdes.2011.06.005.

[45] S. Kumar, J.P. Kruth, Composites by rapid prototyping technology, Mater. Des. 31 (2010) 850–856. doi:10.1016/j.matdes.2009.07.045.

[46] I. Zein, D.W. Hutmacher, K.C. Tan, S.H. Teoh, Fused deposition modeling of novel scaffold architectures for tissue engineering applications, Biomaterials. 23 (2002) 1169–1185.

[47] R.B. Diego, J.M. Estellés, J.A. Sanz, J.M. García-Aznar, M.S. Sánchez, Polymer scaffolds with interconnected spherical pores and controlled architecture for tissue engineering: Fabrication, mechanical properties, and finite element modeling, J. Biomed. Mater. Res. - Part B Appl. Biomater. 81 (2007) 448–455. doi:10.1002/jbm.b.30683.

[48] ISO 604: Plastics—Determination of compressive properties, 2002.

[49] T. Kokubo, H. Takadama, How useful is SBF in predicting in vivo bone bioactivity?, Biomaterials. 27 (2006) 2907–2915.

[50] M.G. Li, X.Y. Tian, X.B. Chen, A brief review of dispensing-based rapid prototyping techniques in tissue scaffold fabrication: role of modeling on scaffold properties prediction., Biofabrication. 1 (2009) 32001. doi:10.1088/1758-5082/1/3/032001.

[51] S.M. Kayhan, A. Tahmasebifar, M. Koç, Y. Usta, A. Tezcaner, Z. Evis, Experimental and numerical investigations for mechanical and microstructural characterization of micro-manufactured AZ91D magnesium alloy disks for biomedical applications, Mater. Des. 93 (2016) 397–408. doi:10.1016/j.matdes.2015.12.177.

[52] ASTM: D 695 – 02a, Standard Test Method for Compressive Properties of Rigid Plastics, 2002.

[53] G. Perego, G.D. Cella, C. Bastioli, Effect of molecular weight and crystallinity on poly (lactic acid) mechanical properties, J. Appl. Polym. Sci. 59 (1996) 37–43.

[54] Y. Shikinami, M. Okuno, Bioresorbable devices made of forged composites of hydroxyapatite (HA) particles and poly- L -lactide (PLLA): Part I . Basic characteristics, Biomaterials. 20 (1999) 859–877.

[55] C.W. Ziemian, M.M. Sharma, S.N. Ziemian, Anisotropic Mechanical Properties of ABS Parts Fabricated by Fused Deposition Modelling, INTECH Open Access Publisher, 2012. doi:10.5772/34233.

[56] B. Ostrowska, J. Jaroszewicz, E. Zaczynska, W. Tomaszewski, W. Swieszkowski, K.J. Kurzydlowsk, Evaluation of 3D hybrid microfiber/nanofiber scaffolds for bone tissue engineering, Bull. Polish Acad. Sci. Tech. Sci. 62 (2014) 551–556. doi:10.2478/bpasts-2014-0059.

[57] K. Auyson, P. Koomsap, A. Chanthakulchan, P. Supaphol, Investigation of applying electrospinning in fused deposition modeling for scaffold fabrication, in: High Value Manuf. Adv. Res. Virtual Rapid Prototyp. Proc. 6th Int. Conf. Adv. Res. Virtual Rapid Prototyping, Leir. Port. 1-5 October, 2013, CRC Press, 2013: pp. 149–155.

[58] J. Korpela, A. Kokkari, H. Korhonen, M. Malin, Biodegradable and bioactive porous scaffold structures prepared using fused deposition modeling, Biomed. Mater. Res. B Appl. Biomater. 101B (2013) 610–619. doi:10.1002/jbm.b.32863.

Figure captions

Figure 1. The FDM machine (Rapman 3.2) used to fabricate PLA scaffolds

Figure 2. The production procedure of PLA/gelatin-forsterite scaffold, fabricated using a combinational approach, 1,2) Fabrication of first and second layers of PLA using FDM, 3) adding nanofibers using ES and 4) adding next layers of PLA using FDM technique

Figure 3. Characterization of PLA scaffolds: SEM images of a) S_1, b) S_2, c) S_3 samples, and d) the cross view the S_3

Figure 4. Stress-strain curves of compression tests performed on PLA samples

Figure 5. Characterization of the PLA/gelatin-forsterite scaffolds: SEM images **(**a) secondary and b) backscatter modes**)** of the PLA/gelatin-forsterite scaffold, c) SEM image of nanocomposite gelatin-forsterite fibrous layer (inset is the TEM micrograph of the forsterite nanopowders) and d) FTIR spectrum of the nanocomposite gelatin-forsterite fibrous layer

Figure 6. Stress-strain of the PLA/gelatin-forsterite scaffold.

Figure 7. Representative SEM images of the PLA/gelatin-forsterite scaffolds after immersion in SBF for 28

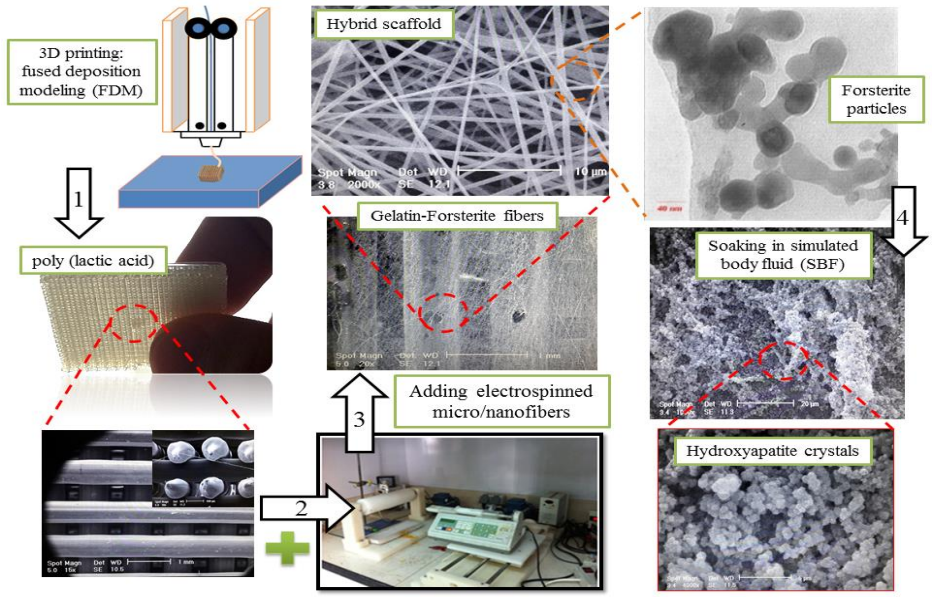

Graphical abstract

Highlights

- Development of newly polymer/ceramic scaffolds consisting of poly(lactic acid) micro-struts and nanocomposite gelatin-forsterite fibrous layers, as a bio-composite.
- Two processing methods, including fused deposition modeling and electrospinning were used to have interconnected pores along with extracellular matrix mimetic structure.
- Using this combinational approach, scaffolds showed a significant increase (about 52%) in the elastic modulus rather than pure ones.
- SEM images confirmed the effects of nanocomposite fibrous layer on the improved bioactivity of the scaffolds.
- These scaffolds showed appropriate mechanical and biological properties for tissue engineering applications, as an extracellular matrix mimetic construct.